Original Article

Integrated UPLC-MS, network pharmacology, and intestinal flora analysis to determine the treatment effect of Qiangzhi decoction on comorbid Tourette syndrome and RRTI

Yunyun Jiang[1], Ting Zhan[1], Mei Wang[2], Yuting Duan[3], Xueqiang Wu[2], Anran Song[2], Jianmin Liu[4], Huishan Shi[1], Chengda Dong[1], Zhaojun Yan[1,4]

[1]College of First Clinical Medical, Shandong University of Traditional Chinese Medicine, Jinan, China; [2]College of Health, Shandong University of Traditional Chinese Medicine, Jinan, China; [3]Department of Traditional Chinese Medicine, Tai'an First People's Hospital, Taian, China; [4]Department of Psychosomatic Medicine, Affiliated Hospital of Shandong University of Traditional Chinese Medicine, Jinan, China

Contributions: (I) Conception and design: Z Yan; (II) Administrative support: Y Jiang; (III) Provision of study materials or patients: T Zhan, Y Duan, X Wu; (IV) Collection and assembly of data: Y Jiang, T Zhan, M Wang; (V) Data analysis and interpretation: A Song, C Dong, H Shi, J Liu; (VI) Manuscript writing: All authors; (VII) Final approval of manuscript: All authors.

Correspondence to: Zhaojun Yan, MD. Department of Psychosomatic Medicine, Affiliated Hospital of Shandong University of Traditional Chinese Medicine, No. 16369 Jingshi Road, Jinan 250014, China; Department of Psychosomatic Medicine, Affiliated Hospital of Shandong University of Traditional Chinese Medicine, Jinan, China. Email: 2020100100@sdutcm.edu.cn.

Background: Tourette syndrome (TS) is a complex neurodevelopmental disorder characterized by vocal and motor tics. Recurrent respiratory tract infection (RRTI), a commonly occurring disease in childhood, correlates with recurrent and severe course of tic symptoms. Qiangzhi decoction (QZD) is a traditional Chinese medicine that can alleviate TS symptoms while reducing the recurrence of RRTI. However, the mechanism of QZD on TS and RRTI remains unclear. This study aimed to determine the treatment effect of QZD on comorbid TS and RRTI by integrating ultrahigh-performance liquid chromatography mass spectrometry (UPLC-MS), network pharmacology, and intestinal flora analysis.

Methods: The components of QZD were first identified by UPLC-quadrupole (Q)-orbitrap-MS/MS. The mechanism of QZD on comorbid RRTI and TS was investigated by a series of network pharmacological methods, including target prediction and bioinformatics analysis. Finally, a comorbid TS and RRTI rat model was established by intraperitoneal injection of 3,3-iminodipropionitrile (IDPN), cyclophosphamide (CTX), and lipopolysaccharide (LPS). Alteration of gut microbiota in the alleviation of TS and RRTI by QZD was investigated via intestinal flora analysis.

Results: The results of UPLC-Q-orbitrap-MS/MS showed that QZD had 96 types of chemical components. The network pharmacology results demonstrated that targets of QZD involved in the treatment of TS and RRTI involved 1045 biological processes (BPs), 109 cellular components (CCs), and 133 molecular functions (MFs), including synaptic and transsynaptic signaling, chemical synaptic transmission, neurotransmitter receptor activity, G protein-coupled amine receptor activity, and serotonin receptor activity, among others. *Firmicutes*, *Bacteroidetes*, *Coprococcus*, and *Lachnospiraceae* played crucial roles in gut microbiota of a QZD-treated comorbid TS and RRTI model.

Conclusions: Our results revealed QZD provided a multicomponent, multitarget, and multipathway synergistic treatment of comorbid TS and RRTI.

Keywords: Qiangzhi decoction (QZD); tourette syndrome (TS); recurrent respiratory tract infection (RRTI); network pharmacology; gut microbiome

Submitted Feb 07, 2023. Accepted for publication Apr 20, 2023. Published online Apr 30, 2023.
doi: 10.21037/atm-23-936
View this article at: https://dx.doi.org/10.21037/atm-23-936

Introduction

Tourette syndrome (TS) is a complex neurodevelopmental disorder characterized by the presence of multiple motor tics and 1 or more phonic tics that last more than 1 year (1). It is reported that its prevalence is between 0.6–1% in school-aged children, and there appears to be no geographical variability (2). The predominant cooccurring comorbid diseases of TS include obsessive-compulsive disorder (OCD), attention deficit hyperactivity disorder (ADHD), and depressive disorder, among others (3). TS is a heterogeneous disease with a multifactorial pathogenesis. The possible pathogenesis of TS is generally considered to be a combination of genetic, immunological, environmental, and psychological factors (4).

In the past 2 decades, the relationship between immune activation, infection, and TS have been widely studied (4-7). These studies focused on infections as a possible contributing factor in TS, particularly those caused by group A Streptococcus (GAS) and mycoplasma pneumonia (MP) (8,9). However, it is unlikely that GAS or MP infections would significantly affect neuropsychiatric symptoms years after their onset. It has been suggested that the immune response may play a triggering role in symptom recrudescence (10).

Recurrent respiratory tract infection (RRTI) is a common disease in childhood and refers to the frequency of upper or lower respiratory tract infections above a certain range in a year (11). Approximately 25% of children under 1 year old have RRTI (12,13), and the incidence shows an increasing tendency (14). Previous study has found that the immune function of children with RRTI was generally weaker than that of normal children, suggesting that abnormal immune function was an important cause of RRTI in children (15). Some studies have demonstrated increased frequency of respiratory infections in TS patients (16,17). A retrospective analysis of 273 children with tics showed that children with RRTI and TS had a higher recurrence rate of tics than children without RRTI, and that children with chronic tics and TS in particular were slower to improve, and RRTI was more likely to recur (17).

Qiangzhi decoction (QZD, patent no.ZL 201310000777.3) is a prescribed Chinese herbal decoction formula. QZD has been widely used for many years to treat TS, achieving remarkable outcomes. In clinical practice, children administered oral QZD showed improvement in tic symptoms along with improvement in RRTI (18). However, there is a lack of systematic and comprehensive research on the mechanism of QZD. Therefore, in this study, we constructed a multilevel network of "prescription-herbal medicine-component-disease-target" to explore the biological mechanism of QZD for TS and RRTI from the perspective of intestinal flora. We present the following article in accordance with the ARRIVE reporting checklist (available at https://atm.amegroups.com/article/view/10.21037/atm-23-936/rc).

Highlight box

Key findings

- Qiangzhi decoction (QZD) provided comorbid Tourette syndrome (TS) and recurrent respiratory tract infection (RRTI) with multicomponent, multitarget therapy and regulated the balance of gut microbiota.

What is known and what is new?

- QZD can ameliorate the tic-like symptoms of TS and reduce recurrence of RRTI.
- QZD can restore the balance of gut microbiota in TS and RRTI model rats.

What is the implication, and what should change now?

- QZD could be a potential therapeutic drug for comorbid TS and RRTI, and the neurotransmitter and immunomodulatory effects need to be further confirmed.

Methods

Materials and reagents

Chromatographic grade of formic acid and methanol and mass spectrometry grade of acetonitrile were purchased from Thermo Fisher Scientific (Waltham, MA, USA). Deionized water was purified by a Milli-Q system (Millipore, Bedford, MA, USA). Microsample total RNA Extraction Kit was purchased from Tiangen Biotech Co., Ltd. (Beijing, China) and TransScript One step gDNA removal and cDNA synthesis Supermix were purchased from Gold Biotechnology Co., Ltd. (Beijing, China).

Preparation of QZD

QZD consists of 7 kinds of traditional Chinese medicine (TCM) herbs (*Table 1*). All herbal plants were purchased from the Affiliated Hospital of Shandong Traditional Chinese Medicine University and in accordance with the standards of Chinese Pharmacopoeia (2020 edition), as

Table 1 Composition of Qiangzhi decoction

Scientific name	Chinese name	Abbreviation	Used plant part	Daily dose of herb (g)	Composition (%)
Morinda officinalis HOW.	Bajitian	MO	Root	9	9.09
Aucklandia lappa Decne	Muxiang	AL	Root	6	6.06
Polygala tenuifolia Willd.	Yuanzhi	PT	Root	9	9.09
Poria cocos (Schw.) Wolf	Fuling	PC	sclerotium	24	24.24
Pinellia ternata (Thunb.) Breit.	Banxia	PB	Root	9	9.09
Atractylodes macrocephala Koidz.	Baizhu	AM	Rhizome	18	18.18
Dioscorea opposita Thunb.	Shanyao	DO	Rhizome	24	24.24

Table 2 Chromatographic gradient

Time (min)	Water phase ratio (%)	Organic phase ratio (%)
1	98	2
5	80	20
10	50	50
15	20	80
20	5	95
27	5	95
28	98	2
30	98	2

confirmed by Professor Li Feng of Pharmacy College, Shandong Traditional Chinese Medicine University. The raw QZD materials were soaked for 1 hour in 10-fold (v/w) the amount of distilled water, followed by decoction for 2 hours. After collecting the filtrates, water was added to the residue (1:8, w/v), and the mixture was extracted with boiling water for another 1.5 hours. The filtrates were mixed and condensed to 0.99 g/mL, and the prepared QZD was stored at −80 ℃ and analyzed using ultrahigh-performance liquid chromatography coupled with quadrupole orbitrap mass spectrometry (UPLC-Q-Orbitrap-MS/MS).

UPLC-Q-orbitrap-MS/MS analysis

For UPLC-Q-Orbitrap-MS/MS analysis, 1,000 µL of 80% methanol was added to 200 µL of the QZD solution and vortexed for 10 minutes. The mixture was then centrifuged at 12,000 rpm for 10 minutes at 4 ℃, after which the supernatant was filtered and analyzed on the machine. The conditions for mass spectrometry were: ion source: electrospray ionization (ESI); scan mode: positive and negative ion switching scan; detection mode: full mass/data-dependent (dd)MS2; resolution: 70,000 (full mass), 17,500 (ddMS2); scan range: 100.0–1,500.0 m/z; spray voltage: 3.2 kV (positive); capillary temperature: 300 ℃; collision gas: high-purity argon (purity ≥99.999%); normalized collision energy (NCE): 30; sheath gas: nitrogen (purity ≥99.999%), 40 arb; auxiliary gas: nitrogen (purity ≥99.999%), 15 arb, 350 ℃; and data acquisition time: 30 minutes. The materials and conditions for chromatographic column were: AQ-C18, 150 × 2.1 mm, 1.8 µm (Welch Materials, Inc., West Haven, CT, USA); flow rate: 0.3 mL/min; aqueous phase: 0.1% formic acid/water solution; organic phase: methanol; eluent: methanol; column oven temperature: 35 ℃; autosampler temperature: 10.0 ℃; and autosampler injection volume: 5.00 µL (see *Table 2* for the gradient elution procedure). SIEVE software version 2.1 (Thermo Fisher Scientific) was used for high-resolution liquid mass spectrometry data acquisition, and retention time correction, peak identification, peak extraction, peak integration, and peak alignment were determined. The data were then searched and compared against the mzCloud database.

Network pharmacology analysis

Construction of "chemical ingredient target"

Based on the experimental results of the UPLC-Q-Orbitrap-MS/MS analysis, PubChem (https://pubchem.ncbi.nlm.nih.gov/) was used to search for the structures of the active compounds of QZD. The obtained structural formula was uploaded to the SwissADME database (http://www.swissadme.ch/) for screening, with the screening parameter for gastrointestinal absorption set at "high". The 2D structure formula of the compound was then

imported into the SwissTargetPrediction database (http://swisstargetprediction.ch/) to predict the target sites, and the output was summarized. Next, the UniProt database (https://www.uniprot.org/) was searched, and the target was transformed into the corresponding standard gene name, which was then sorted out.

Acquisition of "Tourette syndrome" and "RRTI" targets

With "Tourette syndrome" and "recurrent respiratory tract infection" as the retrieval keywords, the related targets of these 2 diseases were found in the following sources: GeneCards database (https://www.genecards.org), DisGeNET database (https://www.disgenet.org), OMIM database (http://omim.org), PharmGkb (https://www.pharmgkb.org/), DrugBank database (https://go.drugbank.com/), and Therapeutic Target Database (http://db.idrblab.net/ttd/). After merging the results and removing duplications, the integrated targets of 6 databases were obtained.

Acquisition of "common targets"

The chemical composition-related targets in Section "Construction of "chemical ingredient target"" and disease targets in Section "Acquisition of "Tourette syndrome" and "RRTI"" targets were uploaded to draw a Venn diagram (https://bioinfogp.cnb.csic.es/tools/venny/) for analysis, and the overlapping genes were obtained as common targets.

Construction and analysis of the protein-protein interaction (PPI) network

The common targets were imported into the String database (https://cn.string-db.org/) to build its PPI using "Homo sapiens" as the selected species. Medium confidence was set to >0.4 to obtain the final intersection targets, and Cytoscape 3.7.2 software was then used to draw the PPI network.

Gene Ontology (GO) analysis and Kyoto Encyclopedia of Genes and Genomes (KEGG) pathway analysis

The target genes were imported into the Database for Annotation, Visualization, and Integrated Discovery (DAVID 6.8, https://david.ncifcrf.gov/), "Homo sapiens" was selected as the species, and KEGG-pathway, GOTERM_BP_DIRECT (BP), GOTERM_CC_DIRECT (CC), and GOTERM_MF_DIRECT (MF) were selected to perform GO and KEGG enrichment analysis of the overlapping genes. We obtained data for the biological processes (BPs), molecular functions (MFs), cellular components (CCs), and the involved pathways to draw GO histograms and KEGG enrichment bubble charts (http://www.bioinformatics.com.cn/).

Animal experiments

Animals

All tests were conducted in accordance with Chinese national laws and local guidelines. A total of 36 healthy male Sprague Dawley (SD) rats (age: 4–7 weeks, weight: 120–150 g) were purchased from Beijing Vital River Laboratory Animal Technology Co. Ltd. (Beijing, China; NO: SCXK 2016-0006) and maintained in plastic cages at 23±2 ℃ with free access to food and water. The rats were exposed to a 12-hour light/dark cycle with their environment maintained at a relative humidity of 30–40%. All animal experiment protocols were conducted in compliance with the National Institute of Health Guide for the Care and Use of Laboratory Animals and were approved by the Animal Ethical Committee of Shandong University of Traditional Chinese Medicine (No. YYLW20222000011). A protocol was prepared before the study without registration. All efforts were made to minimize animal suffering.

TS and RRTI model construction

The study was divided into 5 phases. From days 1–6, the rats underwent adaptive feeding and were provided food and water freely. From days 7–14, the rats were treated with 3,3-iminodipropionitrile (IDPN; Sigma-Aldrich, St. Louis, MO, USA) every 24 hours to induce a TS model (19). From days 15–42, the rats were administered different drugs depending on their treatment group. On days 21, 22, 23, and 27, cyclophosphamide was administered for immunosuppression. On day 42, lipopolysaccharide (LPS) was administered to induce acute lung infection.

The rats were randomly assigned to a control group (CON, n=6) or comorbid TS and RRTI model group (model group, n=30) by using the random number table method. The sample size was empirically estimated. In the model group, rats were injected with IDPN (300 $mg \cdot kg^{-1}$) once daily for 7 days continuously. The control group was injected with an equal volume of 0.9% saline (15 $mL \cdot kg^{-1}$) by intraperitoneal injection. After 7 days of treatment, the model was validated by assessing the rats for typical TS behavior, such as significant head twitching, putting forepaws around the mouth, biting, licking, shaking claws, body raising, or episodic utterance, for longer than

15 minutes in a 30-minute period. Counts were conducted once every 2 weeks by trained observers who were blinded to the group's treatment. All TS model rats were validated in this batch as well as in our pilot observation using an identical protocol.

Subsequently, the rats in the TS model group with IDPN-induced TS were further assigned randomly to 5 groups: model group (model), tiapride hydrochloride and bacterial lysate capsules group (THT-FFS), QZD low-dose group (QZD-L), QZD moderate-dose group (QZD-M), and QZD high-dose group (QZD-H), with each group containing 6 rats. Once a day for 4 weeks, the CON and model group rats were administered normal saline by gastric perfusion at 10 mL/kg, while the QZD-L group received QZD at 2.5 g/kg, the QZD-M group at 5 g/kg, and the QZD-H group at 10 g/kg.

On days 21, 22, 23, and 28, the rats were intraperitoneally injected with CTX (40 mg/kg) for immunosuppression. On day 42, LPS was administered to induce acute lung infection by intraperitoneal injection. Four hours later, all rats were anaesthetized by intraperitoneal injection of 1% sodium pentobarbital (40 mg/kg).

Stool sample collection

Colonic stool samples from the rats were collected into sterile tubes and immediately frozen in liquid nitrogen for intestinal microbiota analysis.

Gut microbiota study

DNA extraction and polymerase chain reaction (PCR) amplification

Three stool samples were selected from each group. Total bacterial DNA was extracted using the Magnetic Soil and Stool DNA Kit (Qiagen, Valencia, California, USA) from fresh stool samples. Based on the manufacture's instructions, the quantity and quality of the extracted DNA were measured using agarose gel electrophoresis. The V3–V4 region of 16S rRNA was amplified by PCR with forward primer CCTAYGGGRBGCASCAG and reverse primer GGACTACNNGGGTATCTAAT. The amplification system was prepared as follows: Phusion Master Mix (2×) (15 μL), Primer F (1 μM) (1 μL), Primers R (1 μM) (1 μL), gDNA (1 ng/μL) (10 μL), and ddH_2O (added to 30 μL). The amplification conditions were initial denaturation at 98 ℃ for 1 minute, then 30 cycles consisting of denaturation at 98 ℃ for 10 seconds, annealing at 50 ℃ for 30 seconds, and extension at 72 ℃ for 30 seconds, with a final extension at 72 ℃ for 5 minutes. The PCR products were recovered and detected by 2% agarose gel electrophoresis to construct the MiSeq library.

High-throughput sequencing

For high-throughput sequencing, libraries were constructed using NEBNext Ultra DNA Library Prep Kit (Illumina, San Diego, CA, USA; E7370L) and tested and quantified by quantitative PCR using Agilent 5400.

Statistical analysis

Windows WPS Office version 11.1.0.13703 was used to summarize data. The topological data were analyzed by Cytoscape version 3.7.2, and pathway enrichment visualization analysis was derived from DAVID version 6.8. For the analysis of gut microbiota, the correlation between factors was calculated by Spearman's rank sum correlation test, and redundancy analysis (RDA) was performed to analyze the correlation between environmental factors and the microbial community. The alpha level was set to P=0.05, and all P values were generated by two-sided tests.

Results

Analysis of chemical components in QZD by UHPLC-Q-Orbitrap-MS/MS

The major compounds in the QZD samples were identified by UHPLC-Q-Orbitrap-MS/MS analysis. The total negative and positive ion chromatograms of QZD (*Figure 1*) demonstrated the chemical composition of all compounds. For full scan experiments, the obtained raw data were preprocessed using SIEVE software, which identified components with mass spectrometric data on experimental and calculated m/z, error in parts per million (ppm), molecular formula, retention time (RT), and MS fragmentation pattern (matched within error tolerance of 25 ppm) with the proposed name of the compounds. As shown in *Table 3*, 96 chemical components were identified in QZD, including 18 carboxylic acids, 13 amino acids, 10 alkaloids, 8 fatty acids, 5 flavonoids, 4 terpenoids, 4 phenylpropanoids, 3 heterocyclic compounds, 3 aldehydes, and 2 amines, among others. The main chemical components were caprolactam, stearamide, 2-anisic acid, citric acid, trigonelline, betaine, formononetin, 5-hydroxymethyl-2-furaldehyde, 4',7-dihydroxyflavanone, and palmitic acid.

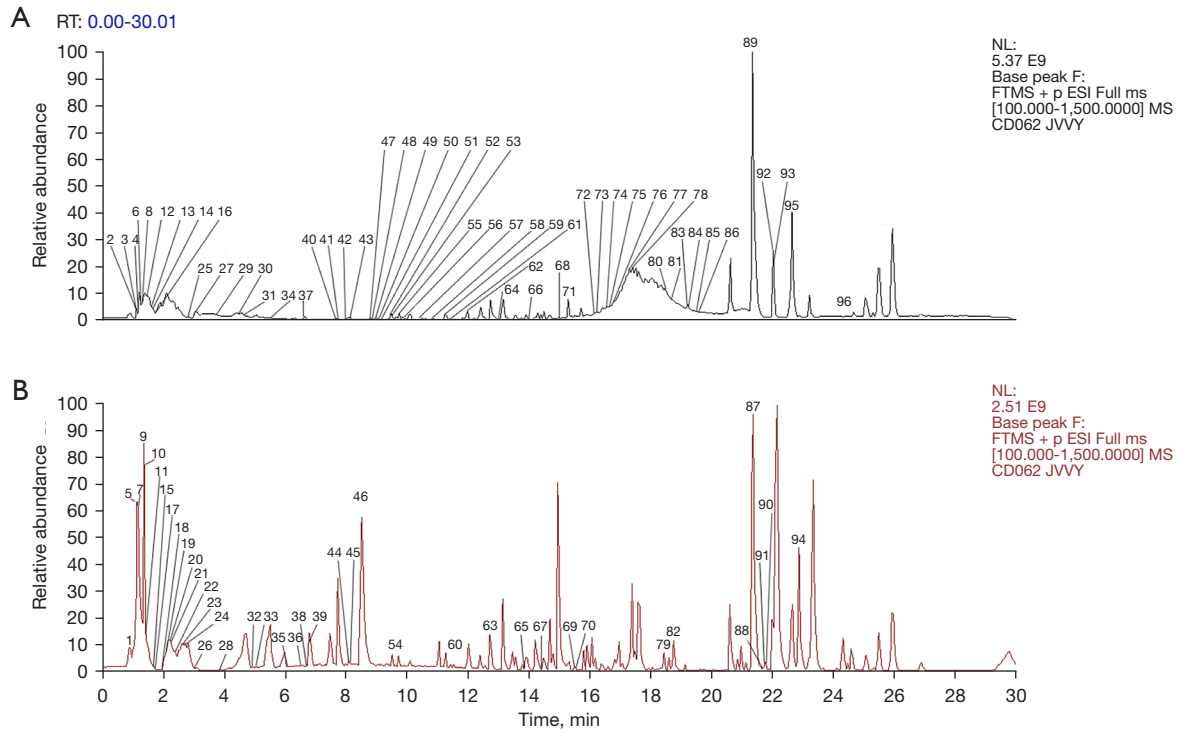

Figure 1 The total ion chromatogram of QZD. (A) The total ion chromatogram of QZD in negative ion mode. (B) The total ion chromatogram of QZD in positive ion mode. QZD, Qiangzhi decoction. RT, retention time; NL, nominal level; FTMS, Fourier transform mass spectrometry; ESI, electrospray ionization.

Mechanism of QZD in treating TS and RRTI based on network pharmacology

Target prediction and screening

As shown in the results of Section "Analysis of Chemical Component in QZD by UHPLC-Q-Orbitrap-MS/MS", 96 chemical components were identified by UHPLC-Q-Orbitrap-MS/MS. In addition, 584 targets were obtained for the chemical components of QZD, as shown in *Figure 2A*.

Using "Tourette syndrome" as the keywords, 177 disease targets were found in DisGeNet, 1,139 in GenCards, 181 in OMIM, 145 in PharmGkb, and 4 in TTD. Using "Recurrence respiratory tract infection" as the keywords, 318 disease targets were found in DisGeNet, 7,826 in GenCards, 73 in OMIM, and 613 in PharmGkb. The targets were then transformed by the UniProt database, and 1,501 TS targets and 8,039 RRTI targets were obtained after removing duplicates. Finally, 848 intersection targets of the 2 diseases were obtained.

As shown in *Figure 2B*, Venn diagram analysis was performed to intersect the disease targets and drug targets, and 102 drug-disease intersection gene targets were obtained.

Construction and analysis of the PPI Network

The targets that acted with active components were submitted to the STRING database to build a PPI network, and protein interaction data with a score > 0.4 was selected (*Figure 2C*). We obtained a total of 102 nodes and 786 edges. The size and lightness of the color of the node indicated the node degree.

Finally, the 20 top targets with the highest nodal degree values were obtained, which were *SLC6A4*, *GRM5*, *SLC6A3*, *GRIN2B*, *CNR1*, *IL6*, *CTNNB1*, *TNF*, *COMT*, *NTRK2*, *DLG4*, *DRD2*, *GRM2*, *IL1B*, *HTR1A*, *HTR2A*, *SLC6A2*, *CHRNA4*, *HTR3A*, and *GRIN1* (*Figure 2D*).

GO enrichment and KEGG pathway analyses

Figure 2C shows the targets of QZD in the treatment of TS and RRTI, reflecting the multiple therapeutic effects of QZD. With P<0.01 and false discovery rate (FDR) <0.01 as the screening criteria, GO analysis showed that the 102 targets of QZD in the treatment of TS and RRTI involved 1,045 BPs, 109 CCs, and 133 MFs.

The BPs of the targets included synaptic and

Table 3 Chemical composition of QZD based on UPLC-Q-orbitrap-MS/MS

No.	RT (min)	Name	ESI	Formula	Molecular weight	Theoretical value (m/z)	Measured value (m/z)	Error (ppm)	Fragmention
1	1.093	DL-Lysine	[M+H]+	C6 H14 N2 O2	146.10563	147.10553	147.10588	2.3949	84.08140
2	1.149	Ornithine	[M-H]-	C5 H12 N2 O2	132.0887	131.08988	131.08882	–8.0680	113.07101
3	1.149	DL-Arginine	[M-H]-	C6 H14 N4 O2	174.11078	173.11168	173.11350	10.5383	131.08145
4	1.154	L-Histidine	[M-H]-	C6 H9 N3 O2	155.06846	154.06948	154.06919	–1.8598	93.04445, 137.03453
5	1.232	L-Cystathionine	[M+H]+	C7 H14 N2 O4 S	222.06735	223.06743	223.06658	–3.8020	88.02207, 134.02727, 206.97220
6	1.285	Threonine	[M-H]-	C4 H9 N O3	119.05697	118.05824	118.05890	5.5637	74.02332, 72.00767, 118.04977
7	1.302	L-Aspartic acid	[M-H]-	C4 H7 N O4	133.03627	132.03751	132.03850	7.5153	88.03903, 115.00248
8	1.31	L-Glutamic acid	[M-H]-	C5 H9 N O4	147.05202	146.05316	146.05424	7.4098	102.05475, 128.03418
9	1.404	Proline	[M+H]+	C5 H9 N O2	115.06363	116.06333	116.06390	4.9238	70.06601
10	1.411	Betaine	[M+H]+	C5 H11 N O2	117.07916	118.07898	118.07843	–4.6460	59.07390, 58.06607
11	1.458	Trigonelline	[M+H]+	C7 H7 N O2	137.04769	138.04768	138.04696	–5.2045	94.06572, 110.06045
12	1.502	D-Raffinose	[M-H]-	C18 H32 O16	504.16906	503.16903	503.16665	–4.7398	89.02305, 59.01242, 179.05545
13	1.64	Gluconic acid	[M-H]-	C6 H12 O7	196.05758	195.05830	195.05720	–5.6533	75.00732, 129.01816, 99.00741
14	1.688	D-(-)-Quinic acid	[M-H]-	C7 H12 O6	192.0628	191.06339	191.06345	0.3240	85.0281
15	1.804	L(-)-Pipecolinic acid	[M+H]+	C6 H11 N O2	129.07923	130.07898	130.07796	–7.8306	84.08147, 70.06596
16	1.846	Glucose 1-phosphate	[M-H]-	C6 H13 O9 P	260.02973	259.02972	259.02846	–4.8604	78.95763, 96.96836
17	1.884	Guanine	[M+NH4]+	C5 H5 N5 O	151.04947	152.04941	152.04795	–9.6008	86.96390
18	1.963	L-Tyrosine	[M+H]+	C9 H11 N O3	181.07419	182.07389	182.07348	–2.2695	91.05498, 136.07527, 123.04450, 80.92865
19	2.162	Nicotinic acid	[M+H]+	C6 H5 N O2	123.03231	124.03203	124.03259	4.5278	–
20	2.229	2-Anisic acid	[M+H]+	C8 H8 O3	152.03176	153.04734	153.04810	4.9389	91.05470
21	2.23	Nicotinamide	[M+H]+	C6 H6 N2 O	122.0483	123.04801	123.04757	–3.5987	80.05016
22	2.387	3-Hydroxy-2-methylpyridine	[M+H]+	C6 H7 N O	109.05321	110.05276	110.05246	–2.7609	82.06574，67.05506, 55.05497
23	2.665	L-Pyroglutamic acid	[M+H]+	C5 H7 N O3	129.04277	130.04259	130.04197	–4.7914	84.04504, 56.05036
24	2.713	L-Norleucine	[M+H]+	C6 H13 N O2	131.09473	132.09463	132.09501	2.8869	86.09718, 60.73380
25	2.822	4-Oxoproline	[M-H]-	C5 H7 N O3	129.04149	128.04259	128.04316	4.4276	84.04392
26	3.057	N-Benzylformamide	[M+NH4]+	C8 H9 N O	118.04211	136.06841	136.06896	4.0133	132.10222, 130.98218, 130.05025, 119.04963
27	3.058	4-Hydroxybenzaldehyde	[M-H]-	C7 H6 O2	122.0372	121.03678	121.03633	–3.7132	93.03329
28	3.756	Uracil	[M+H]+	C4 H4 N2 O2	112.02771	113.02728	113.02706	–1.9232	70.02959, 96.00846

Table 3 (*continued*)

Table 3 (*continued*)

No.	RT (min)	Name	ESI	Formula	Molecular weight	Theoretical value (m/z)	Measured value (m/z)	Error (ppm)	Fragmention
29	3.771	Uridine	[M-H]-	C9 H12 N2 O6	244.06959	243.06954	243.06824	–5.3323	110.02351, 200.05606, 82.02844
30	4.526	Citric acid	[M-H]-	C6 H8 O7	192.0262	191.0270026	191.02890	9.9327	111.0751, 87.00738, 85.02811
31	4.697	Citraconic acid	[M-H]-1	C5 H6 O4	130.02539	129.02661	129.02611	–3.8649	85.02810
32	5.037	6,7-Dihydroxy-4-methylcoumarin	[M+H]+	C10 H8 O4	192.04234	193.04226	193.04277	2.6485	91.05463, 119.04967, 65.03651, 57.27014
33	5.071	Adenosine 3’5’-cyclic monophosphate	[M+H]+1	C10 H12 N5 O6 P	329.0526	330.05252	330.05281	0.8783	136.06195, 57.29844
34	5.495	L-Phenylalanine	[M+NH4]+	C9 H11 N O2	165.07812	166.07898	166.07739	–9.5653	120.08107, 103.05490
35	6.143	5-Hydroxymethyl-2-furaldehyde	[M+H]+	C6 H6 O3	126.03204	127.03169	127.03132	–2.9445	53.03959, 81.03414, 109.02886
36	6.54	N1-Acetylspermine	[M+H]+	C12 H28 N4 O	244.22653	245.22631	245.22581	–2.0452	100.07613, 58.06602, 112.11268
37	6.667	Thymidine	[M-H]-	C10 H14 N2 O5	242.09038	241.09027	241.09189	6.7130	212.89168, 151.05023, 80.96397
38	6.708	N6-Me-Adenosine	[M+H]+	C11 H15 N5 O4	281.11269	282.11240	282.11287	1.6519	150.07730, 162.76067
39	6.814	N,N-Dimethylaniline	[M+H]+	C8 H11 N	121.08941	122.08915	122.08960	3.6911	107.07320, 102.19013
40	7.498	DL-Tryptophan	[M-H]-	C11 H12 N2 O2	204.0894	203.08988	203.08812	–8.6544	116.04935, 74.02332, 142.06517, 159.09183
41	7.722	Methyl 1-(hexopyranosyloxy)-5-hydroxy-7-(hydroxymethyl)-1,4a,5,7a-tetrahydrocyclopenta[c]pyran-4-carboxylate	[M-H]-	C17 H24 O11	404.13206	403.13186	403.13266	1.9805	127.03902, 241.07188, 101.02322
42	7.847	Chlorogenic acid	[M-H]-	C16 H18 O9	354.09541	353.09508	353.09617	3.0809	191.05557, 85.02809
43	7.904	Geniposidic acid	[M-H]-	C16 H22 O10	374.12145	373.12130	373.12417	7.7002	123.04398, 149.05981, 211.06079
44	8.105	5’-S-Methyl-5’-thioadenosine	[M+H]+	C11 H15 N5 O3 S	297.0898	298.08956	298.08800	–5.2351	136.06192
45	8.15	3-Methylbenzophenone	[M+H]+	C14 H12 O	196.08501	197.08882	197.08947	3.3234	105.03400, 84.08159
46	8.529	Caprolactam	[M+H]+	C6 H11 N O	113.08436	114.08406	114.08365	–3.6288	79.05477, 69.07076
47	8.644	Neochlorogenic acid	[M-H]-	C16 H18 O9	354.09541	353.09508	353.09417	–2.5833	191.05553, 135.04407, 179.03436
48	8.661	Shanzhiside methyl ester	[M-H]-	C17 H26 O11	406.15358	405.14751	405.14630	–2.9906	243.08734, 101.02309, 127.03893
49	8.806	Sibiricose A3	[M-H]-	C19 H26 O13	462.1378	461.13734	461.13752	0.3884	137.02333, 461.13077, 93.03323
50	9.121	3-Methylglutaric acid	[M-H]-	C6 H10 O4	146.05693	145.05791	145.05859	4.6961	101.05950, 83.04886
51	9.27	Salicylic acid	[M-H]-	C7 H6 O3	138.03053	137.03169	137.03225	4.0571	93.03320
52	9.414	5-Sulfosalicylic acid	[M-H]-	C7 H6 O6 S	217.9882	216.98851	216.98793	–2.6687	137.02335
53	9.42	Asperulosidic acid	[M-H]-	C18 H24 O12	432.12703	431.12678	431.12975	6.8977	59.01240, 89.02304, 101.02308, 165.05487, 251.05620
54	9.658	Acridine	[M+H]+	C13 H9 N	179.07372	180.07350	180.07299	–2.8282	–

Table 3 (*continued*)

Table 3 (*continued*)

No.	RT (min)	Name	ESI	Formula	Molecular weight	Theoretical value (m/z)	Measured value (m/z)	Error (ppm)	Fragmention
55	9.916	Benzoic acid	[M-H]-	C7 H6 O2	122.03558	121.03678	121.03731	4.3835	–
56	10.135	Isophthalic acid	[M-H]-	C8 H6 O4	166.02565	165.02661	165.02637	–1.4463	121.02830
57	10.429	Caffeic acid	[M-H]-	C9 H8 O4	180.04161	179.04226	179.04333	5.9833	135.04405, 179.03429
58	10.863	Sibiricose A1	[M-H]-	C23 H32 O15	548.17409	547.17412	547.17724	5.7015	205.05017, 223.06088, 164.04703, 265.07214, 59.01240
59	11.401	Cycloolivil	[M-H]-	C20 H24 O7	376.1526	375.15220	375.15532	8.3084	179.07066, 122.03613, 195.06494, 191.07034
60	11.613	5,7-Dihydroxy-4-methylcoumarin	[M+H]+	C10 H8 O4	192.04225	193.04226	193.04279	2.7521	73.49180
61	11.614	3-Coumaric acid	[M-H]-	C9 H8 O3	164.04642	163.04734	163.04804	4.2680	119.04901, 163.03915
62	12.043	Suberic acid	[M-H]-	C8 H14 O4	174.08842	173.08921	173.08809	–6.4644	111.08028, 83.04884
63	12.789	4-Hydroxyephedrine	[M+H]+	C10 H15 N O2	181.09974	182.11028	182.11003	–1.3658	122.09651, 55.93536, 63.92594
64	13.001	4,5-Dicaffeoylquinic acid	[M-H]-	C25 H24 O12	516.12727	515.12678	515.12500	–3.4481	191.05556, 353.08801
65	13.779	4’,7-Dihydroxyflavanone	[M+H]+	C15 H12 O4	256.07351	257.0735589	257.07269	–3.3798	137.02342, 91.98053
66	14.198	Azelaic acid	[M-H]-	C9 H16 O4	188.10412	187.10486	187.10585	5.2965	125.09601, 187.09694
67	14.422	4-Methoxycinnamic acid	[M+H]+	C10 H10 O3	178.05249	179.06299	179.06178	–6.7807	133.06508, 79.05508
68	15.213	Prostaglandin K2	[M-H]-	C20 H30 O5	350.19897	349.20932	349.20886	–1.3289	81.95175
69	15.562	Methyl palmitate	[M+H]+	C17 H34 O2	269.28246	270.25588	270.25673	3.1440	57.07076, 70.06583, 93.49488
70	15.587	7-Hydroxycoumarine	[M+H]+	C9 H6 O3	162.03165	163.03169	163.03294	7.6424	53.03942
71	15.626	Monobutyl phthalate	[M-H]-	C12 H14 O4	222.08912	221.08921	221.08859	–2.7994	71.04878, 121.02829, 59.03314
72	16.157	Corchorifatty acid F	[M-H]-	C18 H32 O5	328.2252	327.22497	327.22790	8.9415	211.13359,171.10187,80.96378
73	16.255	2,3-Dinor prostaglandin E1	[M-H]-	C18 H30 O5	326.19905	325.20932	325.20883	–1.5192	289.18152, 135.08037
74	16.598	Genistein	[M-H]-	C15 H10 O5	270.05272	269.05282	269.05362	2.9607	251.03505, 223.03871
75	16.677	Dodecanedioic acid	[M-H]-	C12 H22 O4	230.15158	229.15181	229.15430	10.8697	211.13364, 167.14334
76	16.803	Formononetin	[M-H]-	C16 H12 O4	268.07357	267.07356	267.07228	–4.7884	269.07867
77	17.316	3-Hydroxyflavone	[M-H]-	C15 H10 O3	238.06282	237.06299	237.06354	2.3024	209.0603
78	17.468	(+/-)9,10-dihydroxy-12Z-octadecenoic acid	[M-H]-	C18 H34 O4	318.24617	317.27082	317.26932	–4.7170	79.95593
79	18.443	7-Methyl-3-methylene-6-(3-oxobutyl)-3,3a,4,7,8,8a-hexahydro-2H-cyclohepta[b] furan-2-one	[M+H]+	C15 H20 O3	248.13045	249.14124	249.14289	6.6047	157.36812
80	18.521	Asiatic acid	[M-H]-	C30 H48 O5	488.35078	487.35017	487.35329	6.3925	469.33405

Table 3 (*continued*)

Table 3 (*continued*)

No.	RT (min)	Name	ESI	Formula	Molecular weight	Theoretical value (m/z)	Measured value (m/z)	Error (ppm)	Fragmention
81	18.701	Rubiadin	[M-H]-	C15 H10 O4	254.05801	253.05791	253.05674	–4.6187	225.05545
82	18.749	Dibutyl phthalate	[M+H]+	C16 H22 O4	278.15165	279.15181	279.15300	4.2659	149.02344, 57.07087
83	19.334	2-(8-Hydroxy-4a,8-dimethyldecahydro-2-naphthalenyl)acrylic acid	[M-H]-	C15 H24 O3	234.16182	251.17254	251.17334	3.1667	80.96381
84	19.335	7-Methylxanthine	[M-H]-	C6 H6 N4 O2	166.04733	165.04908	165.04945	2.2693	149.00861
85	19.547	Hexadecanedioic acid	[M-H]-	C16 H30 O4	286.21478	285.21441	285.21561	4.2094	223.20648, 267.19675
86	19.648	(+/-)12(13)-DiHOME	[M-H]-	C18 H34 O4	314.23537	313.24571	313.24809	7.5993	195.13866, 113.09566, 59.01227
87	21.401	Sedanolide	[M+H]+	C12 H18 O2	194.12	195.13068	195.12930	–7.0712	67.84259
88	21.679	Palmitoyl ethanolamide	[M+H]+	C18 H37 N O2	299.2826	300.28243	300.28389	4.8640	62.06094
89	21.716	α-Linolenic acid	[M-H]-	C18 H30 O2	278.22499	277.22499	277.22771	9.8115	209.11641
90	21.745	Choline	[M+H]+	C5 H13 N O	103.10014	104.10754	104.10756	0.2010	60.08171, 58.06609
91	21.766	Hexadecanamide	[M+H]+	C16 H33 N O	255.25607	256.25621	256.25537	–3.2962	57.07074
92	22.134	Ursolic acid	[M-H]-	C30 H48 O3	456.36082	455.36035	455.36355	7.0375	112.98459
93	22.142	Jasmonic acid	[M-H]-	C12 H18 O3	210.12518	209.12559	209.12490	–3.3206	178.91049, 163.11214
94	22.867	Stearamide	[M+H]+	C18 H37 N O	283.28721	284.28751	284.28480	–9.5495	57.07078
95	22.893	Palmitic acid	[M-H]-	C16 H32 O2	256.24028	255.24023	255.24200	6.9336	94.31187
96	24.314	Stearic acid	[M-H]-	C18 H36 O2	284.27186	283.27153	283.27259	3.7406	–

RT, retention time; ESI, electrospray ionization; QZD, Qiangzhi decoction; UPLC-Q-orbitrap-MS/MS, ultrahigh-performance liquid chromatography coupled ith quadrupole orbitrap mass spectrometry.

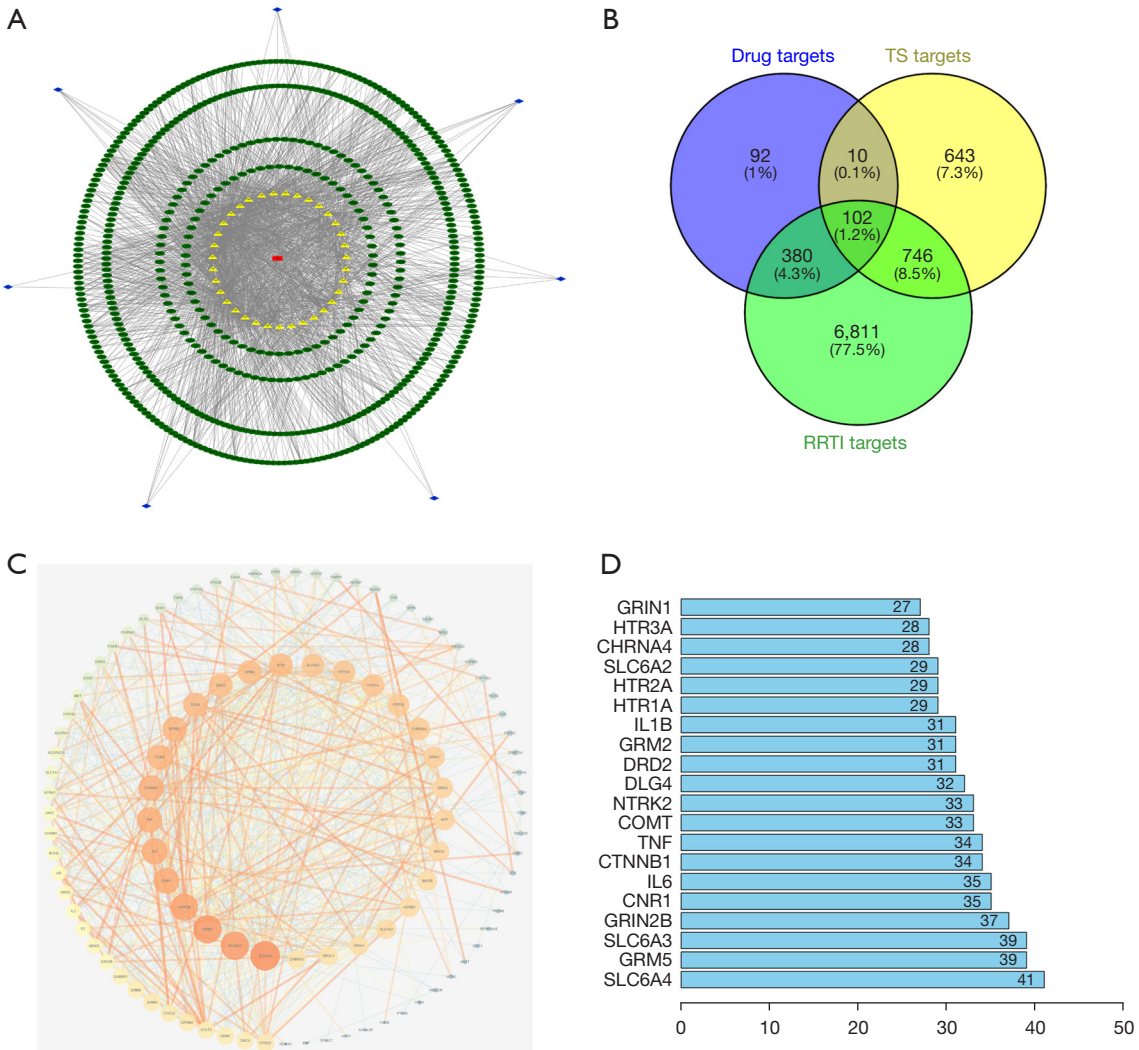

Figure 2 Network pharmacology analysis of QZD. (A) Drug-Herbs-Ingredients-Targets Network. The red rectangle indicates QZD; the blue diamond indicates herbs in QZD; the yellow triangle indicates core ingredients detected by UPLC-Q-Orbitrap-MS/MS; the green circle indicates intersectional targets. (B) Venn diagram depicting all overlaps among the target genes of QZD active targets and the target genes of TS and RRTI. (C) The PPI network of QZD and diseases. The bigger the node size and the denser the color of the node, the more important the gene. (D) Top 20 protein targets. QZD, Qiangzhi decoction; TS, Tourette syndrome; RRTI, recurrent respiratory tract infection; PPI, protein-protein interaction.

transsynaptic signaling, chemical synaptic transmission, regulation of ion transport, regulation of membrane potential, and regulation of secretion (*Figure 3A*).

The CCs included dendrites, synaptic membrane (including presynaptic and postsynaptic membrane), axons, receptor complex, and neuronal cell body (*Figure 3B*).

The MFs included neurotransmitter receptor activity, G protein-coupled amine receptor activity, serotonin receptor activity, amine binding, postsynaptic neurotransmitter receptor activity, and transmitter-gated ion channel activity (*Figure 3C*).

We used DAVID software to obtain 126 KEGG pathways, and 96 pathways had a P value <0.01. As shown in *Figure 3D*, the top 20 signal KEGG pathways included neuroactive ligand-receptor interaction, calcium signaling, neurodegeneration, cAMP signaling, glutamatergic synapse, serotonergic synapse, dopaminergic synapse, and PI3K-Akt signaling.

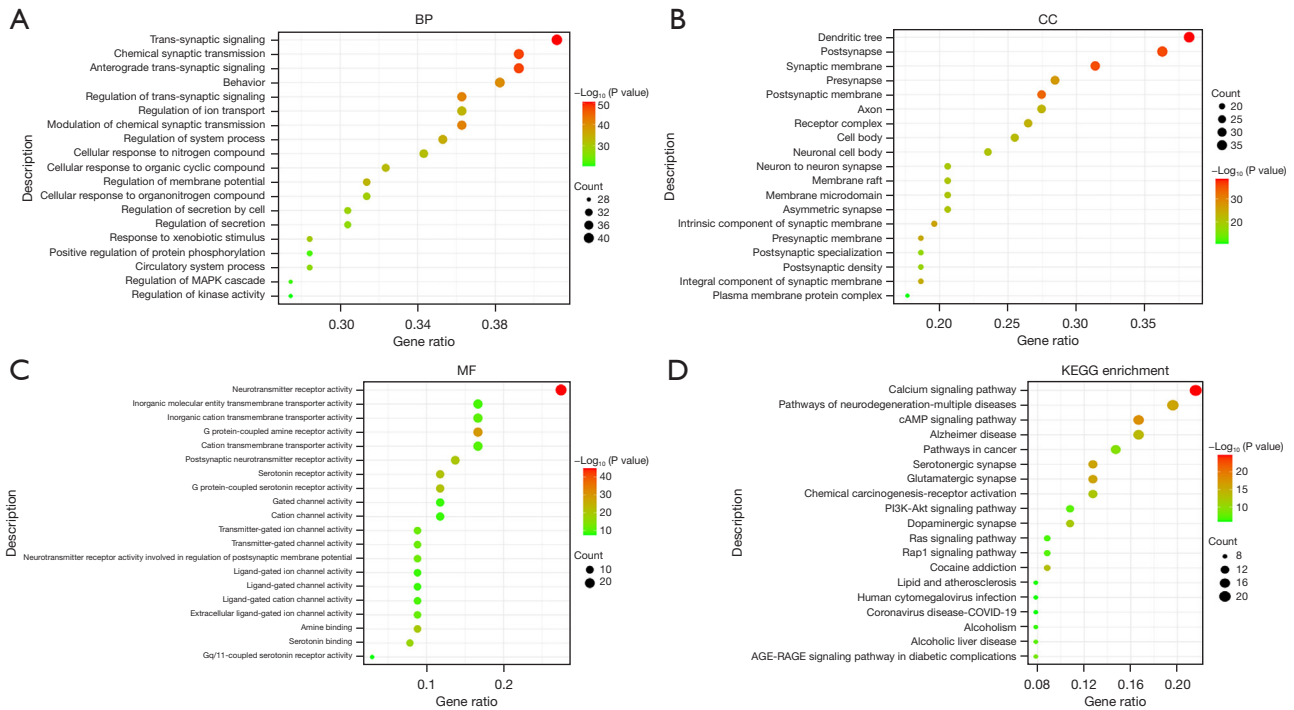

Figure 3 Network pharmacology analysis of QZD. (A) The top 20 GO enrichments in BP. (B) The top 20 GO enrichments in CC. (C) The top 20 GO enrichments in MF. (D) The top 20 KEGG enriched pathways. GO, Gene Ontology; BP, biological process; CC, cellular component; MF, molecular function; KEGG, Kyoto Encyclopedia of Genes and Genomes.

QZD regulated the gut microbiota to remodel gut homeostasis

Three fecal samples from each group were prepared for sequencing to obtain the operational taxonomic units (OTUs). In total, 1173 OTUs were identified at a 97% similarity threshold, 525 of which were detected in all 6 groups (*Figure 4A*). At the phylum level, the relative abundance of *Firmicutes* in the model group was downregulated, while that of *Bacteroidetes* was upregulated (*Figure 4B*). At the family level, the relative abundance of *Enterobacteriaceae* and *Lachnospiraceae* of the model group were significantly lower, whereas that of *Bacteroidetes* family S24-7 OTUs was higher (*Figure 4C*). In the QZD-H, QZD-M, and THT-FFS groups, the relative abundance of these bacteria could be restored to the same level as these of CON group. At the genus level, compared with the CON group, the relative abundance of *Coprococcus* and *Escherichia* in the model group was downregulated (*Figure 4D*). After administration of QZD, the proportions of these 2 genera were increased.

Analysis of alpha diversity indicated species abundance and diversity within a single sample. As shown in *Figure 5A*, the model group's Chao1 index was reduced significantly ($P<0.01$) compared with the CON group, while that of the QZD-H and THT-FFS groups was increased compared with the model group. In addition, the level of Shannon of the model group was lower in microbial communities compared with that of the CON group. Meanwhile, microbial communities showed an increasing trend in the QZD-H and THT-FFS groups (*Figure 5B,5C*), suggesting the gut microbial structural of model rats had been changed, and high-dose QZD treatment increased the diversity of the gut microbiota in TS and RRTI model rats.

Analysis of beta diversity indicated the similarity of microbial composition between groups. A heatmap based on Bray-Curtis is shown in *Figure 5D*. Compared with the CON group, the species composition in the model group was quite different, while the community structure in the QZD-L group was similar.

Linear discriminant analysis effect size (LEfSe) was performed to analyze the differences in community structure between groups to identify differential flora. As shown in *Figure 6A-6D*, compared with the CON group,

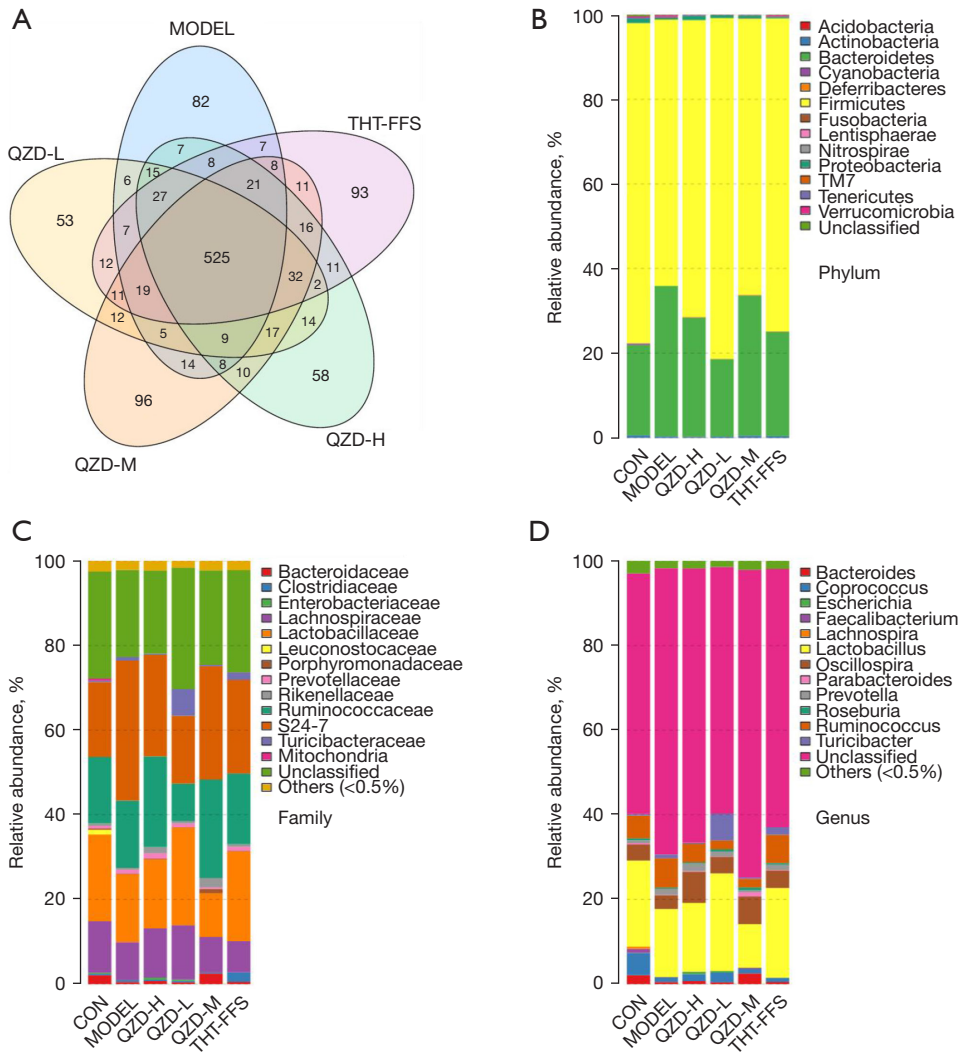

Figure 4 Gut microbiota analysis. (A) Venn diagram of different experimental groups at the OTU level. (B) Histogram of species distribution at the phylum level. (C) Histogram of species distribution at the family level. (D) Histogram of species distribution at the genus level. OTU, operational taxonomic unit; QZD, Qiangzhi decoction; CON, control group; MODEL, model group; THT-FFS, tiapride hydrochloride and bacterial lysate capsules group; QZD-L, QZD low-dose group; QZD-M, QZD moderate-dose group; QZD-H, QZD high-dose group.

Muribaculaceae, *Intestinimonas*, and *Prevotellaceae* were significantly overrepresented in the model group, while in the QZD groups, *Negativicutes*, *Acidaminococcaceae*, *Flintibacter*, *Phascolarctobacterium*, and *Eubacteriaceae* were enriched.

Discussion

Recent studies have reported that infectious agents and the subsequent cerebral immune imbalance appear to be crucial pathological factors in TS (6,20). Recurrent respiratory tract infections are very common in the early years of life, causing significant burden to individuals, families, and society. The coronavirus disease of 2019 (COVID-19) epidemic, caused by *severe acute respiratory syndrome* coronavirus 2 (SARS-CoV-2), continues to spread around the world, and reinfection remains a major challenge in combating COVID-19. Recurrent respiratory infections that may result should be taken seriously. In addition, throughout the epidemic, a surge in tic disorders and TS

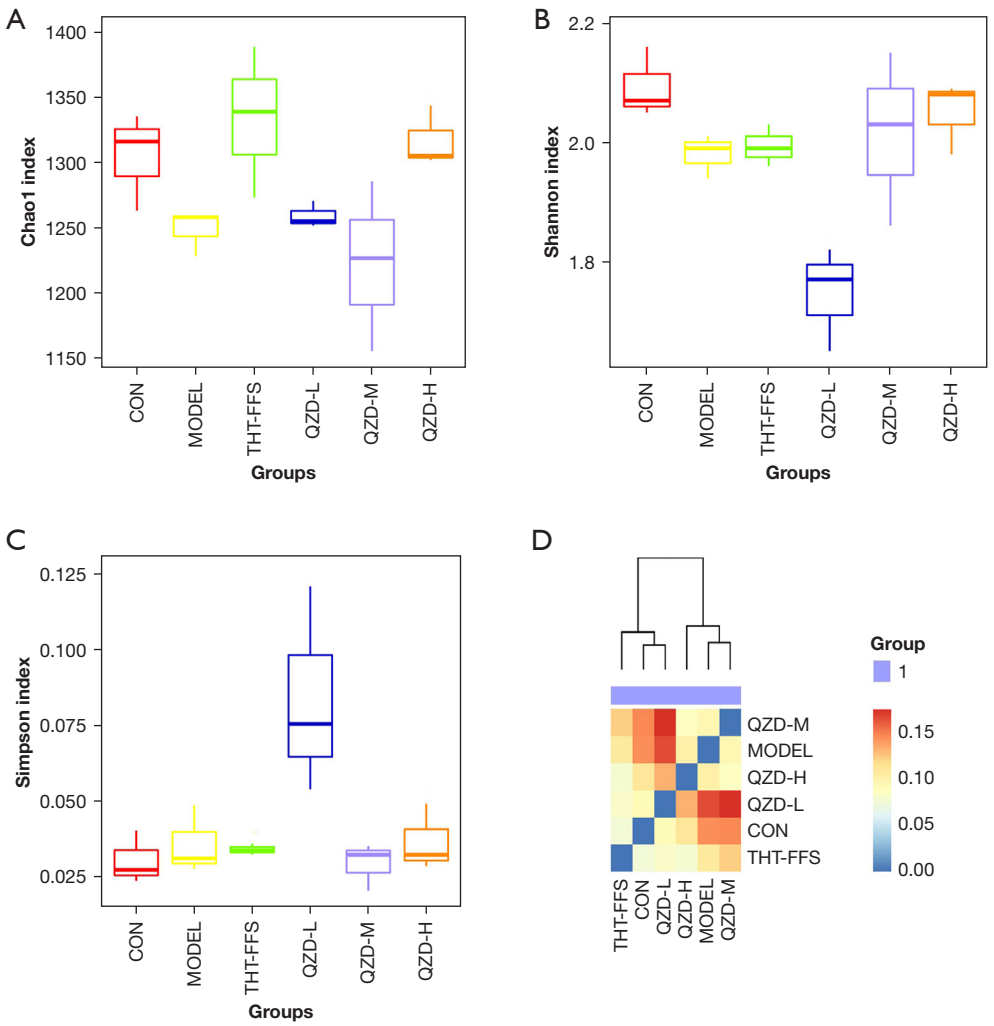

Figure 5 Alpha and beta diversity of gut microbiota analysis. (A) Chao1 index. (B) Shannon index. (C) Simpson index. (D) The heatmap of beta diversity. QZD, Qiangzhi decoction; CON, control group; MODEL, model group; THT-FFS, tiapride hydrochloride and bacterial lysate capsules group; QZD-L, QZD low-dose group; QZD-M, QZD moderate-dose group; QZD-H, QZD high-dose group.

has been reported (21). In light of the simultaneous increase in TS and RRTI, and the clinical relevance, more attention should be given to their cotreatment.

Although TS and RRTI are different diseases, as a fundamental principle of traditional TCM—"treating different diseases with the same treatment"—different diseases with the same pathological basis can follow the same treatment pattern. In accordance with the basic theory of TCM and the Zhiyi Dialectical Theory, the functions of QZD include comforting and strengthening the mind, cultivating the Shen (spirit), and replenishing Zhi (wisdom). Previous study has shown that QZD can significantly reduce tic disorders while also reducing RRTI episodes (18).

The UHPLC-Q-Orbitrap-MS/MS analysis of QZD showed 96 chemical components and 584 drug targets, and 102 intersecting genes were obtained after intersection with disease targets.

The Drug-Herbs-Ingredients-Targets Network demonstrated that most of the compounds display a unique one-to-many pharmacological characteristic, meaning that one compound can act on multiple targets, thereby creating a synergistic effect of multiple therapeutic interventions mechanisms in QZD treatment. In this study, alpha-linolenic acid (Q89) was found to have more targets and is an essential fatty acid with hypolipidemic, anti-inflammatory, anti-tumor, and immune-enhancing effects

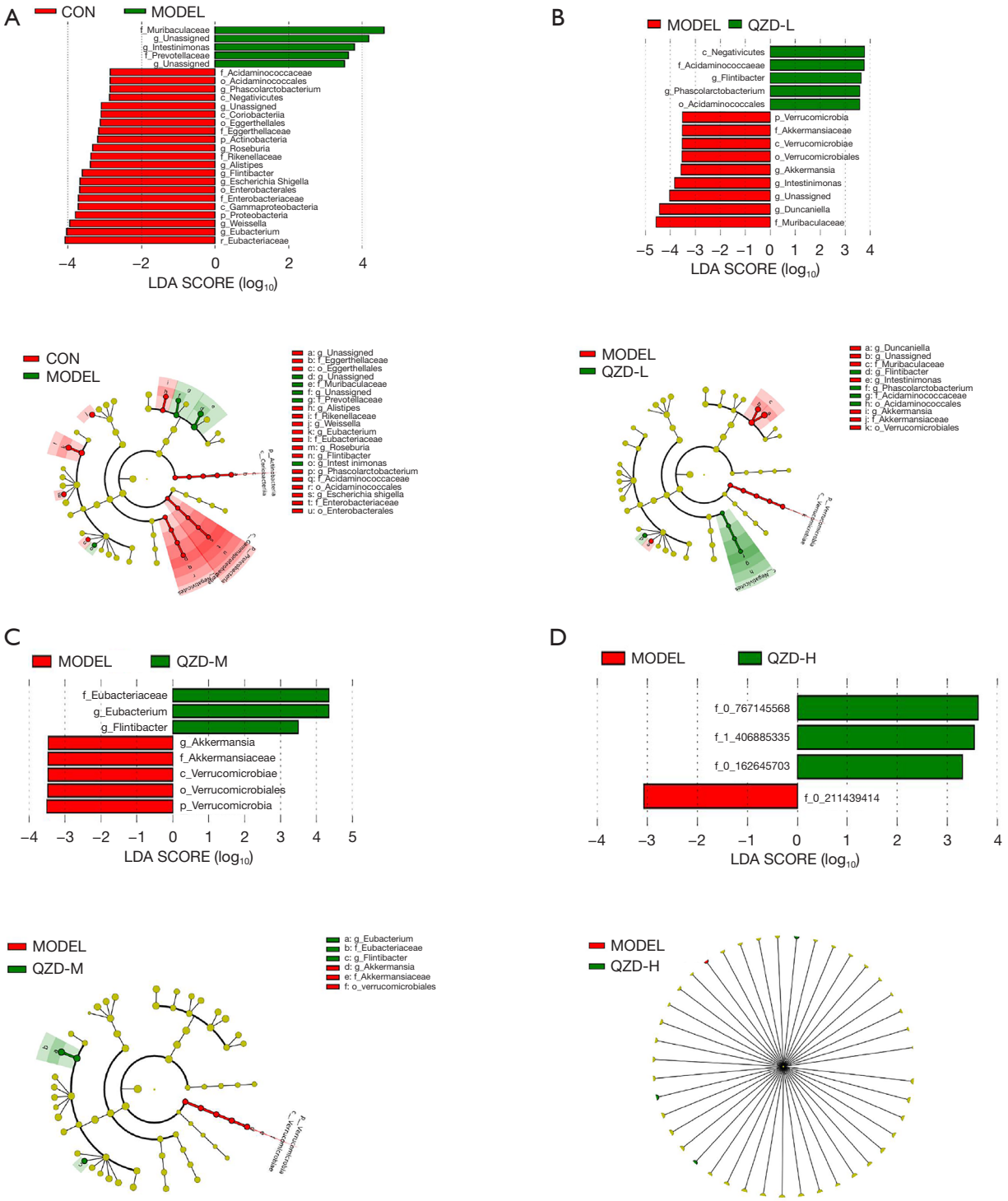

Figure 6 LEfSE diagram comparing gut microbiota between groups. (A) CON group, model group. (B) Model group, QZD-L group. (C) Model group, QZD-M group. (D) Model group, QZD-H group. QZD, Qiangzhi decoction; CON, control group; MODEL, model group; THT-FFS, tiapride hydrochloride and bacterial lysate capsules group; QZD-L, QZD low-dose group; QZD-M, QZD moderate-dose group; QZD-H, QZD high-dose group; LEfSe, Linear discriminant analysis effect size; LDA, Linear Discriminant Analysis.

(22,23); 2-Anisic acid (Q20) was found to possess anti-platelet aggregation effects (24); Jasmonic acid (Q93) has been shown to inhibit pathogenic bacteria, induce the MAP kinase cascade pathway, calcium channels, and interact with numerous signaling molecules (25,26).

Different active ingredients are associated with different numbers of target genes, and the same target can be activated by various types of active ingredients. This suggests that there is a synergistic effect between multiple ingredients in the formula, which may produce synergistic effects through their combined effect on one another.

SLC6A4, one member of the solute carrier family, maps to chromosome 17q11.2 (27). The serotonin transporter (*SERT/SLC6A4*) is an important drug target in the treatment of multiple disorders, including depression, anxiety, autism, TS, and peripherally-based disorders of cardiovascular and gastrointestinal systems.

Interleukin-6 (*IL-6*) has both proinflammatory and anti-inflammatory activities (28,29) and contributes to the transition from acute inflammation to chronic inflammation (30). *IL-6* is a multidirectional cytokine that has important roles in both the immune system and the nervous system, affecting mood, sleep, and neuroimmune regulation, among others. It has been recognized that *IL-6* affects immunity in lung diseases and can also influence the mechanical function of the lung through potential effects on smooth muscle (31).

In this study, the results of GO function and KEGG pathway enrichment analysis found cyclic adenosine 3'5' monophosphate (cAMP), serotonergic, and dopaminergic pathways were associated with QZD in TS and RRTI treatment. As an important second messenger, cAMP is involved in many different cellular activities, acting through cAMP-dependent effectors such as protein kinase A (PKA) and exchange proteins directly activated by cAMP (32). Yang *et al.* (33) found that the cAMP-PKA pathway was involved in the SARS-CoV-2 infection process and induced the activation of the downstream transcription factor cAMP response element-binding protein (CREB). In studies of neuropsychiatric disorders such as TS, abnormalities in second messengers are often found. In postmortem brain samples with TS, Singer *et al.* (34) found mean levels of cAMP reduced in the frontal, temporal, and occipital cortices, and in the putamen. In addition to its key role in human health and medicine, the cAMP signaling pathway is also closely linked to the virulence of fungal plant pathogens, animal pathogens, and *Plasmodium* (35). Liao *et al.* (36) applied *Lactobacillus plantarum* PS128 in the treatment of twitch-like behavior in TS rats, showing that it could reduce cAMP levels in model rats and modulate the phosphorylation of DARPP-32 and thus regulate the intestinal flora.

Dysfunction of the dopaminergic (DA) pathway is associated with tic symptoms in TS (37), which is mainly related to excessive DA innervation (34,38), highly sensitive DA receptors, and presynaptic DA abnormality. Dopamine also plays a major immunomodulatory role, with studies showing dopamine receptors(6,38,39) could be expressed on T cells, B cells, natural killer (NK) cells, and macrophages (39,40). Another study showed that dopamine could be synthesized and stored in follicular helper T cells and released upon cognate interaction with B cells (41). In a study of SARS-CoV-2 infected patients, dopamine biosynthetic enzyme L-Dopa decarboxylase mRNA expression was found to be negatively correlated with SARS-CoV-2 RNA levels, and viral infection downregulated the biosynthetic portion of the dopamine pathway regardless of comorbidities (42).

Serotonin [5-hydroxytryptamine (5-HT)], a fundamental neurotransmitter of the central nervous system, is synthesized from tryptophan (43). 5-HT is produced in the raphe nuclei of the brainstem and is responsible for regulating mood, stress response, sleep, and cognition (8,44). In addition, 5-HT is an important signaling molecule of the peripheral nervous system, especially in the gastrointestinal tract. In some patients with TS, 5-hydroxyindoleacetic acid, a major metabolite of serotonin, has decreased secretion in cerebrospinal fluid, peripheral blood, and 24-hour urine (45). Recent study showed that 5-HT regulates DA neurons through several 5-HT receptors in the brain. Most of the effects of 5-HT on dopamine neurons are indirect, rather than direct effects on DA nerve terminals (46). Peripheral serotonin has been shown to have critical roles in the regulation of both innate and adaptive immune responses (47,48). Recent study found serum serotonin levels might be considered a predictor of outcome in SARS-CoV-2 infection (49).

QZD treatment of TD combined with RRTI has shown to have a positive association with various biological processes and signaling pathways, including trans-synaptic signaling, behavioral changes, chemical synaptic transmission, cellular response to nitrogen compounds, regulation of secretion, and other pathophysiological processes. These clinical benefits are believed to result from the synergy of multiple targets on complex biological processes. The enrichment of different targets in the

same biological process further supports the existence of synergistic actions between multiple targets.

The gut microbiome is a unique symbiotic system within the human body. The "microbiome-gut-brain axis" regulates immune balance, metabolites, and the nervous system through dynamic bidirectional communication. This bidirectional communication can be realized through the interaction of multiple nervous systems, including the central nervous system, the autonomic nervous system, and the enteric nervous system (50). In this regard, gut microbiota can influence host behavior, mood, and cognition by affecting the alteration of neurotransmitters (51). In our study, the intestinal flora of rats in the model group changed significantly compared with that of the CON group. A study of pediatric patients aged 4–8 years with acute onset neuropsychiatric syndrome (PANS) showed changes in abundance of the phylum *Bacteroidetes* and *Firmicutes* compared to a healthy control group (52). A large number of bacteria can manufacture or secrete neurochemicals. For example, *Lactobacillus* and *Bifidobacterium* can secrete gamma-aminobutyric acid (GABA) (53), and *Escherichia* can produce norepinephrine. It has been found that in addition to butyrate production, *Coprococcus* may also be associated with 3,4-dihydroxyphenylacetic acid (DOPAC) production, which is thought to be a dopamine metabolite (54). Dysbiosis of the gut microbiota also affects lung immunity, which in turn affects lung health and respiratory disease. Recent study has found that children with RRTI have significantly fewer numbers of *Bifidobacteria* and *Lactobacilli* and more *Escherichia* in their intestines compared to healthy children (55).

Conclusions

In this study, we analyzed the drug composition of QZD, conducted network pharmacology for comorbid TS and RRTI, and performed intestinal flora analysis, with our results revealing a multicomponent, multitarget, and multipathway synergistic treatment for comorbid TS and RRTI with QZD. Our study provides new insights into the role of QZD in improving comorbid TS and RRTI and identifies potential targets for drug development. However, further studies are needed to confirm this hypothesis.

Acknowledgments

We thank the Experimental Center, Shandong University of Traditional Chinese Medicine for technical support and assistance.

Funding: This work was supported by grants from the National Natural Science Foundation of China (No. 81774249), and Introduce Innovative Teams of 2021 "High School 20 Items" Project (No. 2020GXRC013).

Footnote

Reporting Checklist: The authors have completed the ARRIVE reporting checklist. Available at https://atm.amegroups.com/article/view/10.21037/atm-23-936/rc

Data Sharing Statement: Available at https://atm.amegroups.com/article/view/10.21037/atm-23-936/dss

Peer Review File: Available at https://atm.amegroups.com/article/view/10.21037/atm-23-936/prf

Conflicts of Interest: All authors have completed the ICMJE uniform disclosure form (available at https://atm.amegroups.com/article/view/10.21037/atm-23-936/coif). The authors have no conflicts of interest to declare.

Ethical Statement: The authors are accountable for all aspects of the work in ensuring that questions related to the accuracy or integrity of any part of the work are appropriately investigated and resolved. All animal experiment protocols were conducted in compliance with the National Institute of Health Guide for the Care and Use of Laboratory Animals and were approved by the Animal Ethical Committee of Shandong University of Traditional Chinese Medicine (No. YYLW20222000011).

References

1. Brander G, Isomura K, Chang Z, et al. Association of Tourette Syndrome and Chronic Tic Disorder With Metabolic and Cardiovascular Disorders. JAMA Neurol

2019;76:454-61.
2. Scharf JM, Miller LL, Gauvin CA, et al. Population prevalence of Tourette syndrome: a systematic review and meta-analysis. Mov Disord 2015;30:221-8.
3. Robertson MM, Cavanna AE, Eapen V. Gilles de la Tourette syndrome and disruptive behavior disorders: prevalence, associations, and explanation of the relationships. J Neuropsychiatry Clin Neurosci 2015;27:33-41.
4. Jiang J, Chen M, Huang H, et al. The Aetiology of Tourette Syndrome and Chronic Tic Disorder in Children and Adolescents: A Comprehensive Systematic Review of Case-Control Studies. Brain Sci 2022;12:1202.
5. Tsetsos F, Yu D, Sul JH, et al. Synaptic processes and immune-related pathways implicated in Tourette syndrome. Transl Psychiatry 2021;11:56.
6. Krause DL, Müller N. The Relationship between Tourette's Syndrome and Infections. Open Neurol J 2012;6:124-8.
7. Dale RC. Tics and Tourette: a clinical, pathophysiological and etiological review. Curr Opin Pediatr 2017;29:665-73.
8. Michely J, Eldar E, Martin IM, et al. A mechanistic account of serotonin's impact on mood. Nat Commun 2020;11:2335.
9. Bellanti JA. Recurrent respiratory tract infections in paediatric patients. Drugs 1997;54 Suppl 1:1-4.
10. Eftimiadi C, Eftimiadi G, Vinai P. Staphylococcus aureus Colonization Modulates Tic Expression and the Host Immune Response in a Girl with Tourette Syndrome. Front Psychiatry 2016;7:31.
11. Subspecialty Group of Respiratory Diseases; Society of Pediatrics, Chinese Medical Association; Editorial Board, Chinese Journal of Pediatrics. Clinical concept and management of recurrent respiratory tract infections in children (revised). Zhonghua Er Ke Za Zhi 2008;46:108-10.
12. Chiappini E, Santamaria F, Marseglia GL, et al. Prevention of recurrent respiratory infections : Inter-society Consensus. Ital J Pediatr 2021;47:211.
13. de Benedictis FM, Bush A. Recurrent lower respiratory tract infections in children. BMJ 2018;362:k2698.
14. Cuppari C, Colavita L, Miraglia Del Giudice M, et al. Recurrent respiratory infections between immunity and atopy. Pediatr Allergy Immunol 2020;31 Suppl 24:19-21.
15. Cui QK, Li H, Li Z, et al. Study on the mechanism of the Modified Ginseng-Schisandra Decoction (MGSD) in the treatment of recurrent respiratory tract infection (RRTI) based on network pharmacology. Transl Pediatr 2021;10:1701-11.
16. Kawikova I, Grady BP, Tobiasova Z, et al. Children with Tourette's syndrome may suffer immunoglobulin A dysgammaglobulinemia: preliminary report. Biol Psychiatry 2010;67:679-83.
17. Xin Z, Min W, Ni J, et al. A retrospective analysis on clinical effects of recurrent respiratory infection on "Qufeng Zhidong Decoction"in treating tic disorders. Shanghai Journal of Traditional Chinese Medicine 2015;49:56-8.
18. Ji X, Yan Z. Clinical Study on Qiangzhi Zufang Treating Tic Disorder with recurrent respiratory Tract Infection. Acta Chinese Medicine and Pharmacology 2021;49:72-6.
19. Li Y, Yan Z, Jin Z, et al. Different Doses of IDPN on Tourette Syndrome Rats. Chinese Archives of Traditional Chinese Medicine 2016;34:2442-4.
20. Parker-Athill EC, Ehrhart J, Tan J, et al. Cytokine correlations in youth with tic disorders. J Child Adolesc Psychopharmacol 2015;25:86-92.
21. Horner O, Hedderly T, Malik O. The changing landscape of childhood tic disorders following COVID-19. Paediatr Child Health (Oxford) 2022;32:363-7.
22. Shang X, Yang X, Ding Z. The Intestinal Absorption Characteristics of Compound Safflower Seed Oil were Investigated by Everted Gut Sac Method. Modern Food Science and Technology 2023;39:1-7.
23. Tingting M, Guo H, Linfei J, et al. Extraction and Microencapsulation of Eucommia Seed Oil. Academic Periodical of Farm Products Processing 2012; 10: 81-85+89.
24. Xueying Z, Li L, Kai Y, et al. Clinical observation of Gualou Xiebai Granule in the treatment of PCI postoperative restenosis in soft plaque of coronary artery with syndrome of phlegm-dampness blocking 2017;51:41-4.
25. Dathe W, Rönsch H, Preiss A, et al. Endogenous plant hormones of the broad bean, Vicia faba L. (-)-jasmonic acid, a plant growth inhibitor in pericarp. Planta. 1981;153:530-5.
26. Ruan J, Zhou Y, Zhou M, et al. Jasmonic Acid Signaling Pathway in Plants. Int J Mol Sci 2019;20:2479.
27. Ponleitner M, Szöllősi D, El-Kasaby A, et al. Thermal Unfolding of the Human Serotonin Transporter: Differential Effect by Stabilizing and Destabilizing Mutations and Cholesterol on Thermodynamic and Kinetic Stability. Mol Pharmacol 2022;101:95-105.
28. Tao Y, Xu P, Zhu W, et al. Changes of Cytokines in Children With Tic Disorder. Front Neurol 2021;12:800189.
29. Marcos-Pérez D, Sánchez-Flores M, Proietti S, et al. Association of inflammatory mediators with frailty status

in older adults: results from a systematic review and meta-analysis. Geroscience 2020;42:1451-73.
30. Gabay C. Interleukin-6 and chronic inflammation. Arthritis Res Ther 2006;8 Suppl 2:S3.
31. Rincon M, Irvin CG. Role of IL-6 in asthma and other inflammatory pulmonary diseases. Int J Biol Sci 2012;8:1281-90.
32. Efetova M, Petereit L, Rosiewicz K, et al. Separate roles of PKA and EPAC in renal function unraveled by the optogenetic control of cAMP levels in vivo. J Cell Sci 2013;126:778-88.
33. Yang Q, Tang J, Cao J, et al. SARS-CoV-2 infection activates CREB/CBP in cellular cyclic AMP-dependent pathways. J Med Virol 2023;95:e28383.
34. Singer HS, Hahn IH, Moran TH. Abnormal dopamine uptake sites in postmortem striatum from patients with Tourette's syndrome. Ann Neurol 1991;30:558-62.
35. Borchers A, Pieler T. Programming pluripotent precursor cells derived from Xenopus embryos to generate specific tissues and organs. Genes (Basel) 2010;1:413-26.
36. Liao JF, Cheng YF, Li SW, et al. Lactobacillus plantarum PS128 ameliorates 2,5-Dimethoxy-4-iodoamphetamine-induced tic-like behaviors via its influences on the microbiota-gut-brain-axis. Brain Res Bull 2019;153:59-73.
37. Buse J, Schoenefeld K, Münchau A, et al. Neuromodulation in Tourette syndrome: dopamine and beyond. Neurosci Biobehav Rev 2013;37:1069-84.
38. Minzer K, Lee O, Hong JJ, et al. Increased prefrontal D2 protein in Tourette syndrome: a postmortem analysis of frontal cortex and striatum. J Neurol Sci 2004;219:55-61.
39. Levite M. Dopamine and T cells: dopamine receptors and potent effects on T cells, dopamine production in T cells, and abnormalities in the dopaminergic system in T cells in autoimmune, neurological and psychiatric diseases. Acta Physiol (Oxf) 2016;216:42-89.
40. Arce-Sillas A, Sevilla-Reyes E, Álvarez-Luquín DD, et al. Expression of Dopamine Receptors in Immune Regulatory Cells. Neuroimmunomodulation 2019;26:159-66.
41. Papa I, Saliba D, Ponzoni M, et al. T(FH)-derived dopamine accelerates productive synapses in germinal centres. Nature 2017;547:318-23.
42. Mpekoulis G, Kalliampakou KI, Milona RS, et al. Significance of Catecholamine Biosynthetic/Metabolic Pathway in SARS-CoV-2 Infection and COVID-19 Severity. Cells 2022;12:12.
43. Ye D, Xu H, Tang Q, et al. The role of 5-HT metabolism in cancer. Biochim Biophys Acta Rev Cancer 2021;1876:188618.
44. Kanova M, Kohout P. Serotonin-Its Synthesis and Roles in the Healthy and the Critically Ill. Int J Mol Sci 2021;22:4837.
45. Paschou P, Fernandez TV, Sharp F, et al. Genetic susceptibility and neurotransmitters in Tourette syndrome. Int Rev Neurobiol 2013;112:155-77.
46. Alex KD, Pehek EA. Pharmacologic mechanisms of serotonergic regulation of dopamine neurotransmission. Pharmacol Ther 2007;113:296-320.
47. Shajib MS, Khan WI. The role of serotonin and its receptors in activation of immune responses and inflammation. Acta Physiol (Oxf) 2015;213:561-74.
48. Lin L, Hu K. Serotonin is a multifaceted player in the immune response. Front Biosci (Landmark Ed) 2021;26:253-4.
49. Soria-Castro R, Meneses-Preza YG, Rodríguez-López GM, et al. Severe COVID-19 is marked by dysregulated serum levels of carboxypeptidase A3 and serotonin. J Leukoc Biol 2021;110:425-31.
50. Liang S, Wu X, Hu X, Wang T, Jin F. Recognizing Depression from the Microbiota-Gut-Brain Axis. Int J Mol Sci 2018;19:1592.
51. Mittal R, Debs LH, Patel AP, et al. Neurotransmitters: The Critical Modulators Regulating Gut-Brain Axis. J Cell Physiol 2017;232:2359-72.
52. Quagliariello A, Del Chierico F, Russo A, et al. Gut Microbiota Profiling and Gut-Brain Crosstalk in Children Affected by Pediatric Acute-Onset Neuropsychiatric Syndrome and Pediatric Autoimmune Neuropsychiatric Disorders Associated With Streptococcal Infections. Front Microbiol 2018;9:675.
53. Dinan TG, Stanton C, Cryan JF. Psychobiotics: a novel class of psychotropic. Biol Psychiatry 2013;74:720-6.
54. Valles-Colomer M, Falony G, Darzi Y, et al. The neuroactive potential of the human gut microbiota in quality of life and depression. Nat Microbiol 2019;4:623-32.
55. Li KL, Wang BZ, Li ZP, et al. Alterations of intestinal flora and the effects of probiotics in children with recurrent respiratory tract infection. World J Pediatr 2019;15:255-61.

Cite this article as: Jiang Y, Zhan T, Wang M, Duan Y, Wu X, Song A, Liu J, Shi H, Dong C, Yan Z. Integrated UPLC-MS, network pharmacology, and intestinal flora analysis to determine the treatment effect of Qiangzhi decoction on comorbid Tourette syndrome and RRTI. Ann Transl Med 2023;11(8):299. doi: 10.21037/atm-23-936